

Folding Domain Functions (FDF): a Random Variable Transformation technique for the non-invertible case, with applications to RDEs

Fabrizio Masullo^a, Fabio Zanolin^b, Josep Bonet Avalos^a

^a*Departament d'Enginyeria Química, Escola Tècnica Superior d'Enginyeria Química (ETSEQ),
Universitat Rovira i Virgili, Avda. dels Països Catalans 26, 43007, Tarragona, Spain*

^b*Department of Mathematics, Computer Science and Physics (DMIF), University of Udine, via delle
Scienze 206, 33100 Udine, Italy*

Abstract

The Random Variable Transformation (RVT) method is a fundamental tool for determining the probability distribution function associated with a Random Variable (RV) $Y = g(X)$, where X is a RV and g is a suitable transformation. In the usual applications of this method, one has to evaluate the derivative of $h \equiv g^{-1}$. This can be a straightforward procedure when g is invertible, while difficulties may arise when g is non-invertible. The RVT method has received a great deal of attention in the recent years, because of its crucial relevance in many applications. In the present work we introduce a new approach which allows to determine the probability density function μ_Y of the RV $Y = g(X)$, when g is non-invertible due to its non-bijective nature. The main interest of our approach is that it can be easily implemented, from the numerical point of view, but mostly because of its low computational cost, which makes it very competitive. As a proof of concept, we apply our method to some numerical examples related to random differential equations, as well as discrete mappings, all of them of interest in the domain of applied Physics.

Keywords: Random variable transformation, Distribution function, Density function, Ordinary differential equations, Random differential equations, Non-invertible random transformation, Applications, Numerical simulations

MSC classification: 34F05, 60E05, 65C30.

To Roberto Blanchini, in memoriam

^{*}F.M. acknowledges the Universitat Rovira i Virgili for the Martí i Franquès scholarship 2016 MF-PIPF-27. J.E.

Email addresses: `fabrizio.masullo89@gmail.com` (Fabrizio Masullo), `fabio.zanolin@uniud.it` (Fabio Zanolin), `josep.bonet@urv.cat` (Josep Bonet Avalos)

1. Introduction

The theory of random dynamical systems has been greatly developed in the past fifty years, both from the theoretical and applied point of view [3, 22]. Particularly relevant are the applications to biology, economics and social sciences. More recent applications involve models related to problems in climatology, combustion theory and conduction of electrical impulses in nerve axons [4], just to mention a few examples and to show the great deal of interest in this area of research.

The more general models involve the study of a random differential equations with random initial data, along with the effect of time-dependent noise sources. However, there are many significant examples where such time-dependent noise sources are not present. In these cases, one deals with a deterministic (non-random) law describing the dynamic evolution of the model, where the probabilistic effects only concern the randomness of the initial conditions. In this situation, we can model the dynamic phenomenon as a map which transforms random initial conditions, expressed by a random variable (RV), to an output, whose probability distribution is to be determined [21, Ch.5]. Problems of this kind can be theoretically settled within the framework of the theory of functions of a random variable. More in detail, let X be a random variable, with density function μ_X , defined on a probability space $\Omega = (\Omega, \mathcal{A}, p)$,¹ with values into \mathbb{R} , and let g be a real function defined on \mathbb{R} , which may require some properties that we discuss later on. A classical problem considered in the literature consists in determining the probability distribution of $Y = g(X)$ from the information about X and g . This problem is solved by a standard procedure, by assuming g to be invertible (see [15, p.81]). In particular, in the one-dimensional case, $g : \mathbb{R} \rightarrow \mathbb{R}$, we have a precise formula for the density function μ_Y of Y provided that g is continuously differentiable with a non-vanishing first derivative [15, Corollary 11.2]. A more complex situation arises if g is only piecewise strictly monotone, but continuously differentiable, with a finite set of isolated points where the derivative vanishes, which is the problem that we address in the present article. In this case, if I_1, \dots, I_n is a finite sequence of intervals decomposing the domain of g and such that g is strictly monotone and continuously differentiable in the interior of each interval, we have that

$$\mu_Y(y) = \sum_{i=1}^n \mu_X(h_i(y)) |h'_i(y)| \mathbb{1}_\wedge(y), \quad (1.1)$$

where h_i is the inverse function of g but restricted to the interval I_i , $\wedge = \{y : y = g(x) : x \in \mathbb{R}\}$ and $\mathbb{1}_\wedge(y)$ is the characteristic function which takes a value 1 on \wedge and 0 otherwise (see [15, Corollary 11.3]). Although the formula (1.1) provides a precise definition of the density function associated with the random variable Y , its implementation in concrete

¹As usual, \mathcal{A} denotes a σ -algebra of measurable sets (in the case of our applications \mathcal{A} will denote the collection of Lebesgue measurable sets in \mathbb{R}) and p is a probability defined on \mathcal{A} .

examples can be very difficult. Recent articles applying this method, named *Random Variable Transformation technique*, to different models of present interest in mathematical biology and population dynamics, for instance, deals with more specific situations when g is monotone on its whole domain or has a quadratic shape, thus reducing the complexity only to two symmetric intervals of invertibility (see [8, 7, 10, 5, 6] and the references therein). The aim of this article is precisely to provide the framework to build an efficient algorithm for these cases of interest that cannot be straightforwardly addressed within the standard approach.

A few typical cases, in which a function of a RV may occur in dynamical systems, are the following.

a) As a first example, let us consider the case of a discrete Dynamical System defined by a difference equation of the form

$$x_{n+1} = L(x_n), \tag{1.2}$$

with $L : A \rightarrow A$, where A is a suitable domain in \mathbb{R}^d and L is a sufficiently smooth function. Typical models in population dynamics may involve a non-invertible map L , due to the presence of natural growth restrictions, for instance, of logistic type limitations [19]. The situation becomes even more complicated when we look for periodic points, a problem which is equivalent to the study of fixed points for iterates of L . For a non-invertible L , the shape of the k -th iterate $L^k = \underbrace{L \circ \dots \circ L}_{k \text{ times}}$ can be extremely far from a monotone function.

This is apparent even when studying one-dimensional classical logistic equations (see [18]), as shown in Figure 1 where the logistic map, together with its third iterate, is considered.

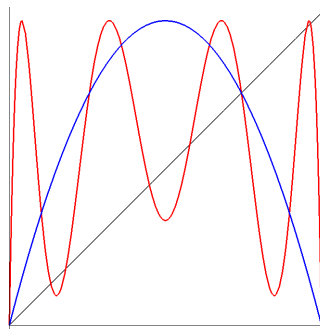


Figure 1: The figure represents the graph of the logistic map $L(x) = rx(1-x)$ and its third iterate $L(L(L(x)))$ in the interval $[0, 1]$. For our example, we have considered the case $r = 3.9$ where there are points of (minimal) period three, as seen from the intersections with the line $y = x$, which is known to yield chaotic dynamics, according to [18].

If we assume that the initial point $x_0 := \phi$ is represented by a RV, we are interested in determining the probability distribution that describes the state of the system after a

certain number k of iterates, or, equivalently, the probabilistic outcome at the k -generation.

b) As a second example, we consider the case of a continuous dynamical system associated with an ordinary differential equation. Here, we are interested in the particular case of a vector system ordinary differential equations of the form,

$$\begin{cases} \frac{d}{dt}\underline{x}(t) = \vec{f}(\underline{x}(t), t) \\ \underline{x}(t_0) = (x_1^0, x_2^0, \dots, x_i^0, \dots, x_d^0) \end{cases} \quad (1.3)$$

where $\underline{x}(t) \in \mathbb{R}^d$. Let us assume that the initial condition $\underline{x}(t_0)$ contains one component, x_r , say, which is a RV, i.e. $x_r^0 = \phi$. If, for a moment, we suppose that $\underline{x}(t_0)$ is a given specific a vector under natural regularity assumptions [14] on \vec{f} , we know that there is a unique solution $\varphi_{\underline{x}(t_0)}(t)$ defined on a maximal interval of existence. Suppose also that for a fixed interval $[t_0, t_1]$, $t_1 > t_0$, all the solutions with initial value $\underline{x}(t_0)$ in a given set D , are defined. In this case, the map $\Psi : \underline{x}(t_0) \mapsto \varphi_{\underline{x}(t_0)}(t_1)$ (the so-called Poincaré map) is a homeomorphism of D onto $\Psi(D)$, as it is well known in the theory of Dynamical Systems. Therefore, if $\underline{x}(t_0) = \phi \in \mathbb{R}$ (i.e. in the one-dimensional case), the map Ψ must be a strictly monotone function, and the RVT method can be straightforwardly applied. However, in all the other situations in which $d > 1$, which are also relevant in Physics, the monotonicity of the maps associated to Ψ is lost.

A significant example comes from the *shooting method*. In this case, we study a second-order scalar differential equation of Newtonian type of the form

$$y''(t) + f(y(t), y'(t), t) = 0, \quad (1.4)$$

corresponding to the planar system

$$\begin{cases} y'(t) = v(t) \\ v'(t) = -f(y(t), v(t), t). \end{cases} \quad (1.5)$$

The initial condition

$$y(t_0) = a, \quad y'(t_0) = b,$$

reads now as

$$y(t_0) = a, \quad v(t_0) = b.$$

Then, to the pair $(a, b) \in \mathbb{R}^2$, we associate the point

$$(a_1, b_1) := \varphi_{(a,b)}(t_1) = (\varphi_{(a,b)}^{(1)}(t_1), \varphi_{(a,b)}^{(2)}(t_1)) \in \mathbb{R}^2,$$

by means of the two-dimensional Poincaré map. Suppose now that for the initial pair (a, b) one of the parameters is determined (for instance the initial position a of the particle), while the other (for instance the initial velocity b) is a RV. In this case, we set $b = \phi$ and,

instead of being interested in the complete map $\varphi_{(a,b)}(t_1)$, we restrict ourselves to the map which associates to ϕ the final position, $\varphi_{(a,\phi)}^{(1)}(t_1)$; this map is not invertible.

In the deterministic case, this procedure consists of fixing the initial position ϕ and look for the final one, given the initial velocity, which needs to be known at the beginning. Then, the probability distribution μ_Y can be reconstructed by *shooting* a bundle of trajectories by varying ϕ , and measuring the density of the end points $y(t)$. We are going to compare the presented algorithm with this simple method, which we will refer to as the *brute-force* algorithm. In this example, we transform the RV ϕ for the initial velocity into a new random variable for the final position at t but the map g describing the transformation is no longer monotone, as one can see from the elementary examples, taken from physical and mechanical models, shown below (see Figure 2 and Figure 3 for two possible cases).

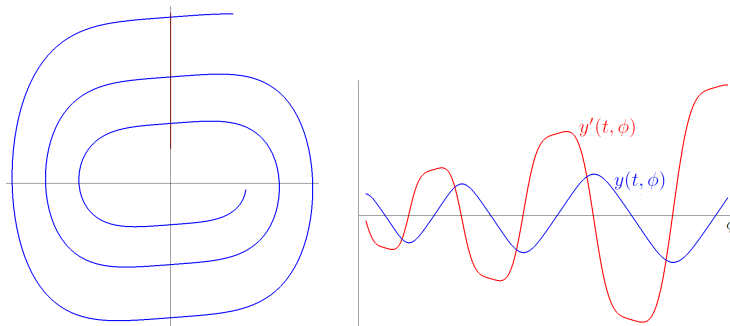


Figure 2: The figure illustrates the use of the shooting method for the Duffing equation, Eq. (1.6).

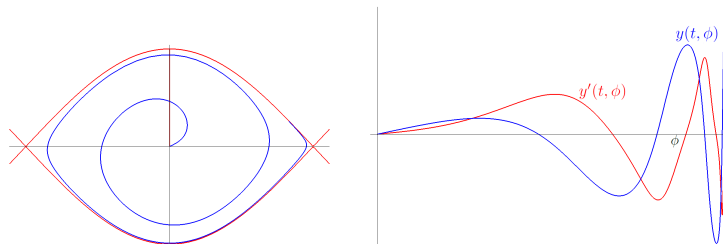


Figure 3: The figure illustrates the use of the shooting method for the pendulum equation, Eq. (1.7).

In Figure 2, we consider the Duffing equation

$$y''(t) + \rho(y(t)) = 0, \tag{1.6}$$

with the superlinear term $\rho(y) = 4y^3$. In this case, it is well-known that the origin is a global center in the phase plane $(y, v) = (y, y')$ and all the orbits around the origin lie on

the energy levels $\frac{1}{2}v^2 + y^4 = \text{constant} > 0$. The left panel shows the image of the Poincaré map after time $t = 10$ of the vertical segment $y(0) = 0, y'(0) = \phi \in [1, 5]$. The right panel shows the graph of the map φ which associates to $\phi \in [1, 5]$ the value of the solutions $y(t, \phi)$, respectively $y'(t, \phi)$, at the time $t = 10$.

In Figure 3, we represent the pendulum equation

$$y''(t) + \sin(y(t)) = 0, \quad (1.7)$$

where the origin is a local center in the phase plane $(y, v) = (y, y')$ bounded above and below by two heteroclinic trajectories. These heteroclinic trajectories connect the unstable equilibrium points $(\pm\pi, 0)$, which represent the geometric configuration of a pendulum going to the inverted vertical position. For an energy constant $0 < c < 2$, all the orbits around the origin lie within the energy levels $\frac{1}{2}v^2 + (1 - \cos(y)) = c$ and are closed curves relatively to the strip $]-\pi, \pi[\times \mathbb{R}$. The left panel shows the image of the Poincaré map after time $t = 20$ of the vertical segment $y(0) = 0, y'(0) = \phi \in]0, 1.998]$. The right panel shows the graph of the map φ which associates to $\phi \in [1, 5]$ the value of the solutions $y(t, \phi)$, respectively $y'(t, \phi)$, at the time $t = 20$.

Both numerical examples above provide simple cases from classical physical problems, in which the map g , is far from being monotone.

c) As a third example, we consider a variant of case *b*), where the dependence of the solution on a random parameter is more involved. We study a second-order problem of the form

$$\begin{cases} y''(t) + f(y(t), y'(t), t) = k\phi \\ y(t_0) = a(\phi), y'(t_0) = b. \end{cases} \quad (1.8)$$

where we have consider a more general dependence on the single random variable other than in the initial conditions, although the RV does not change with time. In this third instance, we can produce very complicated non-monotone maps from apparently rather simple boundary value problems. let us consider harmonic oscillator with constant external force,

$$\frac{1}{\omega^2}y''(t) + y(t) = k\phi \quad (1.9)$$

which produces the mapping

$$\varphi(\phi, t) = k\phi + A \cos(\omega t + \phi). \quad (1.10)$$

In addition, we further assume the following initial conditions

$$y(0) = k\phi + A, \quad y'(0) = 0.$$

This example will be analyzed more in detail in the next section.

Therefore, as we mentioned above, the aim of the present paper is to introduce a new method for the numerical approximation of μ_Y from a given μ_X in cases in which the

theoretical procedure described the formula (1.1) is not effectively applicable. Moreover, we stress that our method can be applied even if we do not have an analytical expression of the function g , which however can be numerically constructed. This is particularly relevant because, in most of the physical applications, the transformation is obtained only in the last way.

Our approach is developed in detail in Section 2. In Section 3 we apply our theory to the example given by (1.10), as a proof of concept. The implemented algorithm is presented in Section 4. Finally, in Section 5 we provide some further numerical examples where we compare our new method, with the application of (1.1) and with the brute force approach. From these examples, the advantage of the new point of view will be evident particularly with respect to the numerical applications.

2. The problem and a fast introduction to FDF

Let us consider an ordinary differential system (like, for instance, (1.5)) where the initial conditions depend on a one-dimensional unknown random number ϕ with mass probability function $\mu : [\alpha, \beta] \subset \mathbb{R} \rightarrow \mathbb{R}$. As a typical application we might consider a projection of the solution onto a one-dimensional subspace, thus obtaining a new mass probability distribution function (PDF) $\psi(y, t)$ that evolves in time. That is, we look for the PDF $\mu_Y := \psi(y, t)$ that describes the probability of finding our system in the position y at time t , provided that we know the probability distribution $\mu_X := \mu(\phi)$.

For each $\phi \in [\alpha, \beta]$, the (projected) deterministic solution of the differential equation is a function $\varphi_\phi(t) : [0, t_{max}] \rightarrow \mathbb{R}$ that describes how the system evolves in time t . Under standard smoothness conditions on the vector field (cf. [14]) the function $\varphi(\phi, t) := \varphi_\phi(t)$ is of class $\mathcal{C}^1([\alpha, \beta] \times [0, t_{max}])$. As we have discussed in the introduction, for any fixed $t > 0$, the map $\phi \mapsto \varphi_\phi(t)$ may be non-invertible. The idea behind the present work is that the evolution in space $y(t) = \varphi(\phi, t)$ of the system, spreads, squeezes or stretches and overlaps or folds the probability mass $\mu(\phi)$ in the space. Then we propose to replace the representation of the physical system given by $\varphi(\phi, t)$, with a new mathematical entity, which we call *folding domain function FDF*, such that we can determine $\psi(y, t)$ with the minimum computational cost. Although in the present demonstration the FDF method is applied assuming that we already know the analytical solution φ of the mapping, this does not affect the applicability of the FDF algorithm (FDF-A) to cases where the differential system is not analytically solvable, but a suitable approximation to the solution can be obtained from *numerical integrators*. As a matter of fact, the FDF-A algorithm only requires the knowledge of a finite set of values $\varphi_i := \varphi(\phi_i, t)$ (with $i \in \{1, \dots, N_{div}\}$ and $N_{div} \in \mathbb{N}$), for some initial conditions $\phi_i \in [\alpha, \beta]$, which contain all the relevant information for the mapping and that we will define later on. Interestingly, these particular values can be determined from the knowledge of the analytical solution of the differential equation but, more important, from the application of any numerical solver of the initial value problem.

2.1. The folding domain functions

Let X be a RV defined on a probabilistic measure space with values in a compact interval $[\alpha, \beta]$ and let $g : [\alpha, \beta] \rightarrow [g_{\min}, g_{\max}]$ be a continuously differentiable function which is strictly piecewise monotone. Accordingly, we decompose the domain of g into a finite sequence of adjacent intervals, by setting

$$\alpha = \alpha_0 < \alpha_1 < \cdots < \alpha_{j-1} < \alpha_j < \cdots < \alpha_k = \beta,$$

with the convention that g is strictly monotone with nonzero derivative on each subinterval $]\alpha_{j-1}, \alpha_j[$ and, moreover, each α_j with $0 < j < k$ is a stationary point which is a strict local maximum or local minimum. Let also

$$A := \{\alpha_j : j = 0, \dots, k\}.$$

Notice that, by construction, the map g is strictly increasing/decreasing restricted between two consecutive points in A . It will be also convenient to introduce the following notation

$$\begin{cases} A_j := [\alpha_{j-1}, \alpha_j[& \text{for } j = 1, \dots, k-1 \\ A_k := [\alpha_{k-1}, \alpha_k] = [\alpha_{k-1}, \beta], \end{cases}$$

so that the intervals A_j ($j = 1, \dots, k$) determine a partition of the interval $[\alpha, \beta]$.

We define the vector $\Lambda := (\lambda_1, \dots, \lambda_k)$, where, for each $j = 1, \dots, k$, we set

$$\lambda_j := g(\alpha_j) - g(\alpha_{j-1})$$

(see Figure 4 for an illustrative example). We also introduce the constant

$$S = S_\Lambda := \sum_{j=1}^k |\lambda_j|.$$

As a next step, we define the transformation $\hat{g} : [\alpha, \beta] \rightarrow [0, S]$ as

$$\begin{cases} \hat{g}(x) = m_{j-1} + |g(x) - g(\alpha_{j-1})|, & \text{for } x \in [\alpha_{j-1}, \alpha_j] \\ j = 1, \dots, k, \end{cases} \quad (2.1)$$

where

$$m_0 = 0 \quad \text{and} \quad m_j := |\lambda_1| + \cdots + |\lambda_j|, \quad j = 1, \dots, k.$$

By definition, $\hat{g}(\alpha) = 0$ and $\hat{g}(\beta) = S$. The formula (2.1) defining \hat{g} is introduced as a way to unfold the graph of g . Indeed, transformation \hat{g} acts as follows: given a graph of a piecewise monotone function g , first we shift it as to have value 0 at $x = \alpha$. Then, if $[\alpha_{j-1}, \alpha_j]$ is an interval where g is increasing, we further shift this portion of the graph of g by the quantity $m_{j-1} - g(\alpha_{j-1}) = |\lambda_1| + \cdots + |\lambda_{j-1}| - g(\alpha_{j-1})$. On the other hand, if

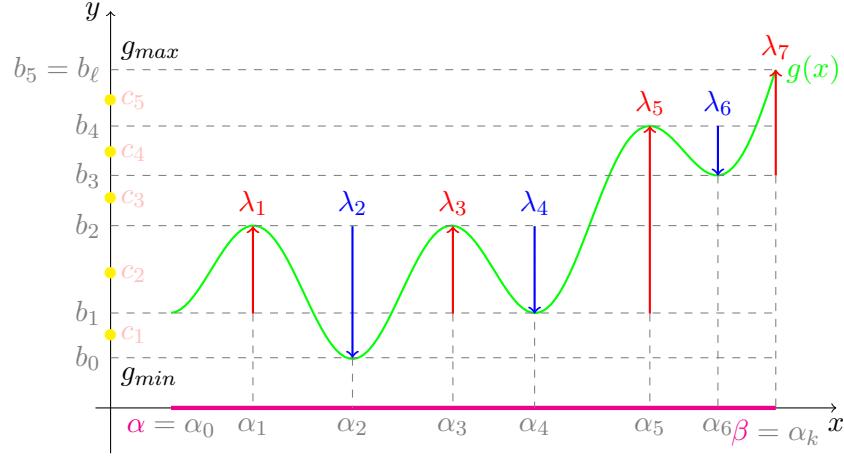


Figure 4: The function g .

$[\alpha_{j-1}, \alpha_j]$ is an interval where g is decreasing, we reflect the graph of g symmetrically with respect to the horizontal line $y = g(\alpha_{j-1})$ and then we shift it as to obtain the graph of a continuous and monotonously increasing function (see Figure 5 for an illustrative example). Observe that, if g is smooth (of class C^1), \hat{g} is smooth, too.

By construction, for any continuously differentiable and piecewise monotone function $g : [\alpha, \beta] \rightarrow [g_{\min}, g_{\max}]$ we have that $\hat{g} : [\alpha, \beta] \rightarrow [0, S]$ is strictly monotonously increasing with inflection points at α_i ($i = 1, \dots, k-1$) and, moreover,

$$\frac{d}{dx} \hat{g}(x) = \left| \frac{d}{dx} g(x) \right|, \quad \forall x \in [\alpha, \beta].$$

At this point, the inverse function of \hat{g} is well defined as

$$\eta : [0, S] \rightarrow [\alpha, \beta].$$

This new map is again strictly monotonously increasing and continuously differentiable on $[0, S] \setminus \{\hat{g}(\alpha_i), i = 1, \dots, k-1\}$, where the derivative in the excluded points exists with value $+\infty$ (see Figure 6).

Let us consider the set

$$B = \{g(\alpha_i), i = 0, \dots, k\} = \{b_0, b_1, \dots, b_\ell\},$$

with $g_{\min} = b_0 < b_1 < \dots < b_\ell = g_{\max}$

and decompose $[g_{\min}, g_{\max}]$ into non-overlapping sets B_i as

$$[g_{\min}, g_{\max}] = B_1 \cup B_2 \cup \dots \cup B_\ell,$$

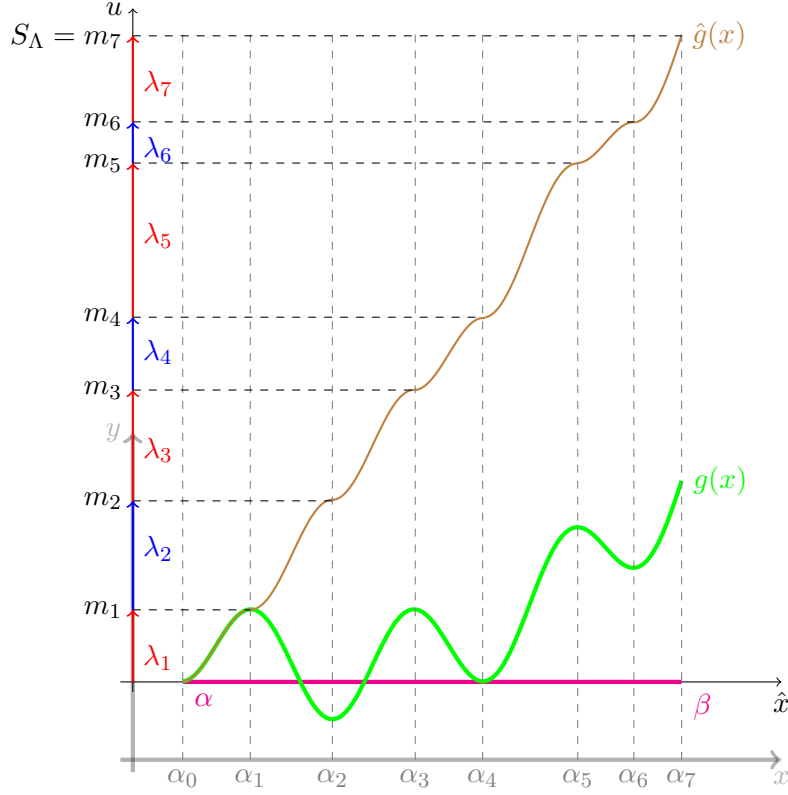


Figure 5: The functions g and \hat{g} .

where

$$\begin{cases} B_i := [b_{i-1}, b_i[, & \text{for } i = 1, \dots, \ell - 1 \\ B_\ell := [b_{\ell-1}, b_\ell] = [b_{\ell-1}, g_{\max}]. \end{cases}$$

Note that for each $y \in [g_{\min}, g_{\max}]$ there is a (nonempty) finite set of points in the inverse image $g^{-1}(\{y\}) \subset [\alpha, \beta]$. Thus the (finite) set of indexes

$$I(y) := \{j \in \{1, \dots, k\} : \exists x \in A_j : g(x) = y\}$$

is well defined.

Lemma 2.1. *If $W \subset [\alpha, \beta]$ is an open interval such that $g(W) =]b_{i-1}, b_i[$ for some $i \in \{1, \dots, \ell\}$, then g is strictly monotone in W .*

Proof. For the proof it is sufficient to observe that, by our assumption, the only possible critical points of g are contained in the set A . On the other hand, $B = g(A)$ and $]b_{i-1}, b_i[\subset$

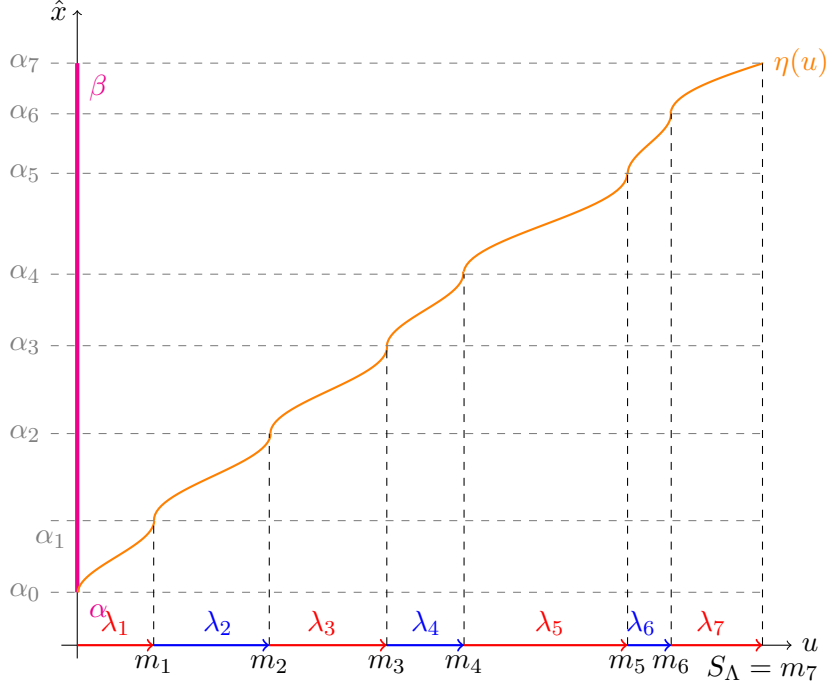


Figure 6: The function η .

$[g_{\min}, g_{\max}] \setminus B$. As a consequence, $g'(x) \neq 0$ for all $x \in W$ and therefore, g is strictly monotone in W . \square

Lemma 2.2. *For each $y \in]b_{i-1}, b_i[$ (where $i \in \{1, \dots, \ell\}$ an arbitrary index), the set $I(y)$ is constant. Therefore, $I(y) = I(c_i)$ where $c_i := \frac{b_{i-1} + b_i}{2}$.*

Proof. For a fixed $i \in \{1, \dots, \ell\}$, let us consider the middle point $c_i := \frac{b_{i-1} + b_i}{2}$ and let $\gamma_1 < \gamma_2 < \dots < \gamma_p$ be such that $g^{-1}(\{c_i\}) = \{\gamma_1, \dots, \gamma_p\}$. For each γ_s , with $s = 1, \dots, p$, let W_s be an open maximal interval containing γ_s and such that $g(W_s) =]b_{i-1}, b_i[$. By Lemma 2.1, g is strictly monotone on W_s and, therefore, the open intervals W_s are pairwise disjoint. In fact, if, by contradiction, two of these intervals, say W_s and W_r , overlap, then $W_s \cup W_r$ turns out to be a unique interval W such that $g(W) =]b_{i-1}, b_i[$ and hence g must be strictly monotone on W , contradicting the fact that $g(\gamma_s) = g(\gamma_r) = c_i$ (with $\gamma_s \neq \gamma_r$). As a consequence of the fact that the open intervals are pairwise disjoint, we conclude that

$$g^{-1}(]b_{i-1}, b_i[) = W_1 \cup \dots \cup W_p$$

and then

$$\#g^{-1}(\{y\}) = \text{constant}, \quad \forall y \in]b_{i-1}, b_i[,$$

where $\#E$ denotes the cardinality of the set E (in our case it is just the number of points, as all the involved sets are finite).

As a final observation, we claim that each of the intervals W_s is contained in exactly one of the intervals A_j . Indeed, let $r \in \{1, \dots, p\}$ be such that $W_r \subset]\alpha_{j-1}, \alpha_j[$ and let $s \neq r$. If, by contradiction, also $W_s \subset]\alpha_{j-1}, \alpha_j[$, then $\gamma_r, \gamma_s \in]\alpha_{j-1}, \alpha_j[$ with $\gamma_r \neq \gamma_s$ and $g(\gamma_r) = g(\gamma_s) = c_i$, contrary to the fact that g is strictly monotone on $A_j = [\alpha_{j-1}, \alpha_j]$.

This latter observation guarantees that $I(y)$ is constant for each $y \in]b_{i-1}, b_i[$ and the proof is complete. \square

Remark 2.1. It is interesting to observe that the result about the constancy of $\#g^{-1}(\{y\})$ for all $y \in]b_{i-1}, b_i[$ is a general property which is valid also for locally invertible and proper maps on metric spaces, as proved in [2, §3].

As a next step we want to introduce a formal method to determine, for a given $y \in [g_{\min}, g_{\max}]$, the set $I(y)$. We will treat separately the case when $y = b_i$, or $y \in]b_{i-1}, b_i[$ (for some $i \in \{1, \dots, \ell\}$). The first situation concerns the analysis of a finite set and will be treated in a second moment. Concerning the second case, by virtue of Lemma 2.2, it will be sufficient to consider $I(c_i)$, where c_i is the middle point of each interval. It is straightforward to check that $y \in]g(\alpha_{j-1}), g(\alpha_j)[$ (when $g(\alpha_{j-1}) < g(\alpha_j)$) or, respectively $y \in]g(\alpha_j), g(\alpha_{j-1})[$ (when $g(\alpha_{j-1}) > g(\alpha_j)$), provided that

$$0 < (y - g(\alpha_{j-1}))\text{sign}(\lambda_j) < |\lambda_j|, \quad (2.2)$$

a condition which can be easily implemented from an algorithmic point of view. To better understand the meaning of (2.2), recall that $\text{sign}(\lambda_j)$ determines whether g is increasing or decreasing on each interval $[\alpha_j, \alpha_{j+1}]$.

Since the map g is (in general) non-invertible, the idea now is to spread the point y on the interval $[0, S]$, which is the range of the function \hat{g} and the domain of the function η , in such a way that, at each $y \in]b_{i-1}, b_i[$, we associate a set of points

$$u_{\rho_1}(y), u_{\rho_2}(y), \dots, u_{\rho_p}(y), \quad \text{for } I(y) = \{\rho_1, \rho_2, \dots, \rho_p\}.$$

More precisely, we obtain these values by setting

$$u_j(y) = m_{j-1} + (y - g(\alpha_{j-1}))\text{sign}(\lambda_j), \quad \text{for } j \in I(y). \quad (2.3)$$

Then, by means of the inverse mapping η , we can obtain the set of points of the initial domain which share the same image y . More formally, we have that

$$x_j(y) = \eta(u_j(y)) = \left(g|_{] \alpha_{j-1}, \alpha_j[}\right)^{-1}(y), \quad \text{for } j \in I(y).$$

which is the collection of points in the domain of g that share the same image. In conclusion, via the function η we obtain a cumulative inverse of all the local inverse functions of g restricted to the single intervals A_j , where g is strictly monotone.

We summarize the procedure described above, by recalling the previous diagrams. We start in Figure 4 from a function g where we split its domain into a finite number of adjacent intervals where g is either strictly increasing or strictly decreasing. On the vertical axis we have also indicated the set of points $B = \{b_0, \dots, b_\ell\}$ which is the set $\{g(\alpha_0), \dots, g(\alpha_k)\}$ with its elements arranged in the natural order. The figure also provides a visual illustration of Lemma 2.2. Indeed, it is apparent that $I(y)$ is constant and equal to $I(c_i)$ for each $y \in]b_{i-1}, b_i[$. The same figure also puts in evidence the vector $\Lambda = (\lambda_1, \dots, \lambda_k)$.

Figure 5 illustrates the transformation $g \mapsto \hat{g}$ and reports the starting coordinate system (x, y) and the translate (\hat{x}, u) , which shifts $g(\alpha_0)$ to 0. The figure also puts in evidence the new special points m_i on the u -axis.

Finally, Figure 6 shows the graph of the function $\eta = \hat{g}^{-1}$. As explained theoretically above, for any given image y we have a method to “invert” the function g via the function η , provided that we correctly associate the set of points $u_j(y)$ for $y \in I(y)$ to $y \in [g_{\min}, g_{\max}]$

It remains to discuss the case when $y \in B$, namely when $y = b_i$ for some $i = 0, \dots, \ell$. We recall that for these points, it may exist $x_j(y)$ such that $g'(x_j(y)) = 0$. The fact that the $\#B$ is finite assures that these points are irrelevant in probability theory as they represent an ensemble of zero measure. However, we provide a more detailed demonstration for completeness.

We start by mentioning again that $\#g^{-1}(\{y\})$ is constant only on $]b_i, b_{i+1}[$ (according to Lemma 2.2), but it changes at the ends of the interval. In general, the set $g^{-1}(\{b_i\})$ contains at least a critical point α_j (with $j = 1, \dots, k - 1$) or an extreme point α_j (with $j = 0, k$) and, possibly other points in the interior of the intervals A_j where g is strictly monotone. This situation is evident from the example in Figure 4: the $g^{-1}(\{b_3\})$ contains a regular point and a critical point of minimum; When we increase y passing across b_3 , we find $1 - 2 - 3$ solutions. On the other hand, the set $g^{-1}(\{b_4\})$ contains a regular point and a critical point of maximum and then, when we increase y passing across b_4 , we find $3 - 2 - 1$ solutions. This example reflects a general situation and suggests the need to distinguish, among the critical points, the strict local minima and the strict local maxima. This intuitive explanation is now formalized in what follows.

We split $g^{-1}(\{b_i\})$ as

$$g^{-1}(\{b_i\}) = \mathcal{C}_m^i \cup \mathcal{C}_M^i \cup \mathcal{R}^i \cup \mathcal{E}_m^i \cup \mathcal{E}_M^i,$$

where \mathcal{C}_m^i and \mathcal{C}_M^i denote the sets of critical points which are interior strict local minima or strict local maxima, respectively, while \mathcal{R}^i is the set of regular points in the interior of the interval. We denote by \mathcal{E}_m^i and \mathcal{E}_M^i the sets of extreme points $\{\alpha, \beta\}$ (having b_i as image) which are, respectively, local minima or local maxima. Now the rule to count the number of inverse images passing from an interval $]b_{i-1}, b_i[$ to the next one $]b_i, b_{i+1}[$ across the point b_i is given by:

$$\#I(c_{i+1}) = \#I(c_i) + 2\#\mathcal{C}_m^i - 2\#\mathcal{C}_M^i - \#\mathcal{E}_M^i.$$

Respectively, the rule passing from an interval $]b_i, b_{i+1}[$ to the previous one $]b_{i-1}, b_i[$ across the point b_i is given by:

$$\#I(c_i) = \#I(c_{i+1}) - 2\#\mathcal{C}_m^i + 2\#\mathcal{C}_M^i - \#\mathcal{E}_m^i.$$

Conversely, if we know the type of the points in $g^{-1}(\{b_i\})$, we can determine the number of elements of $I(y)$ for y in an interval having b_i as an extremal point. In fact, the following holds:

$$\#I(y) = \#g^{-1}(\{b_i\}) + \#\mathcal{C}_m^i - \#\mathcal{C}_M^i - \#\mathcal{E}_M^i, \quad \forall y \in]b_i, b_{i+1}[.$$

To justify the above formula, we observe that if $b_i = g(\alpha_j)$ (for some $j = 1, \dots, k-1$), where α_j is an interior point of strict local minimum, then for $\varepsilon > 0$ and sufficiently small we have exactly two points $x_{j,\text{left}} < \alpha_j < x_{j,\text{right}}$ in a (small) neighborhood of α_j such that $g(x_{j,\text{left}}) = g(x_{j,\text{right}}) = y$. If $b_i = g(\alpha_j)$ (for $j = 0, k$) is the image of an extreme point which is a local minimum, then there is exactly one point \tilde{x} in a right neighborhood of α (respectively in a left neighborhood of β) such that $g(\tilde{x}) = y$. If $b_i = g(x^*)$ for some $x^* \in \mathcal{R}^i$, we have that g is strictly monotone (increasing or decreasing) in an open interval containing x^* and therefore there exists a unique point in such an open interval having y as image. Finally, if $b_i = g(\alpha_j)$ for some $j = 0, \dots, k$ with α_j a point of local maximum (in the interior or at the boundary of $[\alpha, \beta]$), there are no solutions of $g(x) = y$ in a neighborhood of α_j . In this manner we have counted all the possible solutions of $g(x) = y \in]b_i, b_i + \varepsilon[$ for $\varepsilon > 0$ and sufficiently small. Taking into account that the number of these solutions is constant in the open interval $]b_i, b_{i+1}[$ we have proved the above formula.

In a similar manner we prove that

$$\#I(y) = \#g^{-1}(\{b_i\}) - \#\mathcal{C}_m^i + \#\mathcal{C}_M^i - \#\mathcal{E}_m^i, \quad \forall y \in]b_{i-1}, b_i[.$$

As a final step, we propose a visual description (see Figure 7) to detect the inverse images of a point $y \in [g_{\min}, g_{\max}]$ using the components of the vector Λ and the set $I(y)$.

Our procedure consists in starting from the point $g(\alpha_0) = b_{i^*} \in B$ (for some $i^* \in \{1, \dots, \ell\}$) and superimpose suitable *layers* by taking $\lambda_1, \dots, \lambda_k$. All the points b_i are obtained as points of the form

$$b_{i^*} + \lambda_1 = g(\alpha_1), \quad b_{i^*} + \lambda_1 + \lambda_2 = g(\alpha_2), \quad \dots, \quad b_{i^*} + \sum_{j=1}^k \lambda_j = g(\alpha_k) = g(\beta).$$

Once the points $g(\alpha_j)$ are arranged in the natural order for the set B , as $\{b_1, \dots, b_\ell\}$, for any fixed $\bar{y} \in]b_{i-1}, b_i[$, in order to determine the set $I(y)$, we have just to look for the number of layers meeting the vertical line $y = \bar{y}$ (as observed above in Lemma 2.2, we can take $\bar{y} = c_i$). The corresponding scheme is illustrated in Figure 7 below. For the figure we take as a function g , the one reported in Figure 4.

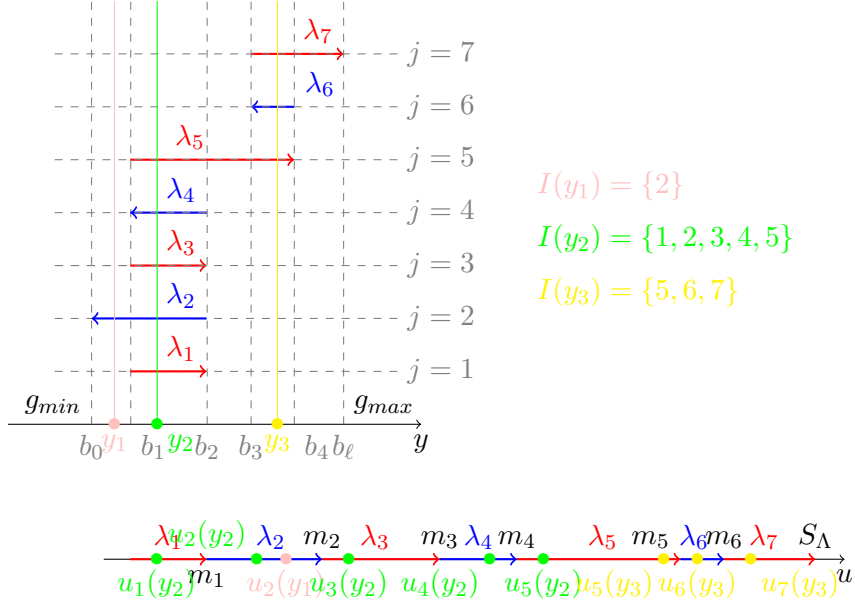


Figure 7: The layers.

Remark 2.2. In the sequel we will apply the method described above to maps obtained from a class of random dynamical systems. In this case, the function g comes from a map $\varphi(x, t)$, for a fixed value of the time t . The derivative of the auxiliary function η will determine the density of a composite RV. From a topological point of view, the evolution of $\varphi(x, t)$, as t varies in a time-interval, can be interpreted as sequence of functions $g_t(x)$ which transform (fold) the RV X (with values in $[\alpha, \beta]$) and mass probability function μ_X into a new RV $Y_t = g_t(X)$. In this perspective, it is natural to consider the above method as a technique which at any time t “unfolds” the range $[g_{\min}, g_{\max}]$ of g to the new range $[0, S_\lambda]$ which becomes the new domain of the function η , as shown in the example of Figure 7.

2.2. The connection with the theory of Random Variable Transformation

Let X be a RV with range in a compact interval $[\alpha, \beta]$ and let $g : [\alpha, \beta] \rightarrow [g_{\min}, g_{\max}]$ be a smooth and piecewise monotone function as it is the one constructed in Section 2.1. Our goal is to show that the FDF is consistent with the general theory which provides the probability distribution function of the new RV $Y = g(X)$.

Using the same notation as in the previous section, given any $\tilde{y} \in]b_{i-1}, b_i[$ and a sufficiently small $\varepsilon > 0$ such that

$$]\tilde{y} - \varepsilon, \tilde{y} + \varepsilon[\subset]b_{i-1}, b_i[,$$

according to Lemma 2.2 we have that the set of indices $I(y)$, representing the layers associated with y , is constant for all $y \in]\tilde{y} - \varepsilon, \tilde{y} + \varepsilon[$. Thus,

$$\begin{aligned}
P(\tilde{y} - \varepsilon < Y < \tilde{y} + \varepsilon) &= P(X \in g^{-1}(] \tilde{y} - \varepsilon, \tilde{y} + \varepsilon [)) \\
&= \sum_{j \in I(\tilde{y})} P(X \in (g|_{A_j})^{-1}(] \tilde{y} - \varepsilon, \tilde{y} + \varepsilon [)) \\
&= \sum_{j \in I(\tilde{y})} P(X \in \eta(] u_{j,\min}(\tilde{y}), u_{j,\max}(\tilde{y}) [)) \\
&\quad u_{j,\min}(\tilde{y}) := \min\{u_j(\tilde{y} - \varepsilon), u_j(\tilde{y} + \varepsilon)\}, \\
&\quad u_{j,\max}(\tilde{y}) := \max\{u_j(\tilde{y} - \varepsilon), u_j(\tilde{y} + \varepsilon)\} \\
&= \sum_{j \in I(\tilde{y})} \int_{\min\{u_j(\tilde{y}-\varepsilon), u_j(\tilde{y}+\varepsilon)\}}^{\max\{u_j(\tilde{y}-\varepsilon), u_j(\tilde{y}+\varepsilon)\}} \mu_X(\eta(u)) \eta'(u) du \\
(*) &= \sum_{j \in I(\tilde{y})} \int_{\tilde{y}-\varepsilon}^{\tilde{y}+\varepsilon} \mu_X(\eta(u(\xi))) \eta'(u(\xi)) \left| \frac{du(\xi)}{d\xi} \right| d\xi \\
(*) &= \sum_{j \in I(\tilde{y})} \int_{\tilde{y}-\varepsilon}^{\tilde{y}+\varepsilon} \mu_X((g|_{A_j})^{-1}(\xi)) \left| \frac{d}{d\xi} (g|_{A_j})^{-1}(\xi) \right| d\xi.
\end{aligned}$$

where, in this equation g^{-1} does not strictly stand for the inverse of g , which generally speaking is not invertible, but it represents the collection of pre-images of the segment $] \tilde{y} - \varepsilon, \tilde{y} + \varepsilon [$. In contrast, $(g|_{A_j})^{-1}$ represents the actual local inverse of the segment for the set A_j . Moreover, in the last two steps (indicated by $(*)$), we have used the fact that

$$\eta'(u(y)) \left| \frac{du(y)}{dy} \right| = \left| \frac{d}{dy} (g|_{A_j})^{-1}(y) \right|$$

and also that in fact, $\frac{du(y)}{dy} = \pm 1$.

On the other hand, by definition,

$$P(\tilde{y} - \varepsilon < Y \leq \tilde{y} + \varepsilon) = \int_{\tilde{y}-\varepsilon}^{\tilde{y}+\varepsilon} \mu_Y(\xi) d\xi.$$

Therefore, comparing the two expressions, we obtain that

$$\mu_Y(y) = \sum_{j \in I(y)} \mu_X((g|_{A_j})^{-1}(y)) \left| \frac{d}{dy} (g|_{A_j})^{-1}(y) \right|, \quad (2.4)$$

holds for all $y \in [g_{\min}, g_{\max}] \setminus B$. In this manner, we have reestablished (1.1), for $h_i := (g|_{A_j})^{-1}$ indicating that the FDF method is consistent with the general theory for the RVT. Eq. (2.4) also holds for the segment end points $y = g(\alpha_0) = g(\alpha)$ (respectively,

for $y = g(\alpha_k) = g(\beta)$ provided that they are not a *critical value*. The formula is not applicable to the critical values b_0, \dots, b_ℓ because for these points the derivative of the inverse function is infinite. Notice that such a limitation is also present in the general RVT theory as expressed in (1.1). However, in our situation, as the number of critical values is finite the ensemble of critical points of g in the interval $[\alpha, \beta]$ is thus a set of zero measure. Therefore, the weight of the critical values is negligible in the computation of the cumulative distribution function F_Y , provided that X is a continuous RV or a discrete/mixed one with a finite number of jumps at points which are not critical. Finally, in the very special case in which there are jumps for the RV X at some critical points of g , the problem will be solved by a direct computation as a limit from the neighboring compact environment.

3. An example

In order to demonstrate the applicability of the method, we start with a concrete example. Let us assume that our RDE admits an analytical solution $y(t) := \varphi(\phi, t)$. For example, recalling that the RDE Eq. (1.9) leads to solutions of the form (1.10), we assume that our physical system evolves according to:

$$\varphi(\phi, t) := k \cdot \phi + A \cdot \cos(\omega t + \phi), \quad (3.1)$$

Where $k > 0$ is a given constant, $A > 0$ is the *amplitude*, $\omega > 0$ is the *angular frequency*, and ϕ is the *initial phase*. Furthermore we assume that $\phi = X$ is a random number that belongs to the interval $[\alpha, \beta]$. We suppose that ϕ has mass probability function:

$$\mu_X : [\alpha, \beta] \subset \mathbb{R} \rightarrow \mathbb{R}. \quad (3.2)$$

In each fixed time instant $t = t^* > 0$ the physical system is in the position $y(t^*) = \varphi(\phi, t^*)$ and such a position depends on the particular initial phase $\phi \in [\alpha, \beta]$. We notice that, from the mathematical point of view, $y = \varphi(\phi, t)$ is a scalar field $\varphi : [\alpha, \beta] \times [0, t_{max}] \subset \mathbb{R}^2 \rightarrow \mathbb{R}$ that associates to each element (ϕ, t) a point y in the real physical space. Our idea is that, in each instant of time $t^* \in [0, t_{max}]$, we can get the probability mass function $\mu_Y := \psi(y, t^*)$ for the variable $y(t^*)$ by applying the new formal concept introduced above. We start by replacing the physical map given by Eq. (3.1) by the FDF, motivated by the theoretical results of the previous section. In Figure 8 we report the plot of the functions (3.1), corresponding to the physical solution in the (ϕ, t) plane (yellow), together with (3.2), giving the probability distribution of the random variable X . On the right-hand side of the figure we have singled out three instants of time $0 < t_1^* < t_2^* < t_3^* < t_{max}$, to show that the problem depends on the final time chosen for the analysis. In each of these times, we plot a function $g_{t_i^*} : [\alpha, \beta] \subset \mathbb{R} \rightarrow \mathbb{R}$ ($i \in \{1, 2, 3\}$), such that:

$$\begin{aligned} g_{t_1^*}(\phi) &:= \varphi(\phi, t_1^*), \\ g_{t_2^*}(\phi) &:= \varphi(\phi, t_2^*), \\ g_{t_3^*}(\phi) &:= \varphi(\phi, t_3^*). \end{aligned}$$

We notice that each of these three functions maps the interval $[\alpha, \beta]$ on the $x = \phi$ -axis in a non-bijective way to the y -axis. As explained, we proceed to the separation of $g_{t_i^*}(\phi)$ into all the monotone pieces as we vary ϕ from α to β , as we described. Second, we identify the increasing from the decreasing pieces to construct $\hat{g}_{t_i^*}(\phi)$. As each of these pieces are invertible, we can calculate the transformation of μ_X into the *unfolded intermediate* $\tilde{\mu}_Y^t$, with $t = t_1^*, t_2^*, t_3^*$. Then, following the indicated procedure, we construct the final folded μ_Y . The key element is to realizing that the *folding* process will introduce the overlap of the different sections. In Figure 8 we show precisely the overlapping pieces that will give rise to the final μ_Y .

In more detail, for each $t = t_1^*, t_2^*, t_3^*$ we have a different vector $\Lambda = \Lambda_t$ which collects all the needed set of information to construct the functions \hat{g} , η and the associated layers. For $t = t_1^*$, in Figure 8 the first arrow is a blue arrow that corresponds to the first decreasing part of $g_{t_1^*}$. The second is a red arrow that corresponds the increasing part of $g_{t_1^*}$ and the last one is another blue arrow that corresponds to the also decreasing part of $g_{t_1^*}$. We proceeded similarly for $g_{t_2^*}$ and $g_{t_3^*}$. Observe that, as the time varies, the corresponding Λ_t changes and, therefore, the size and direction of the *arrows*, as well.

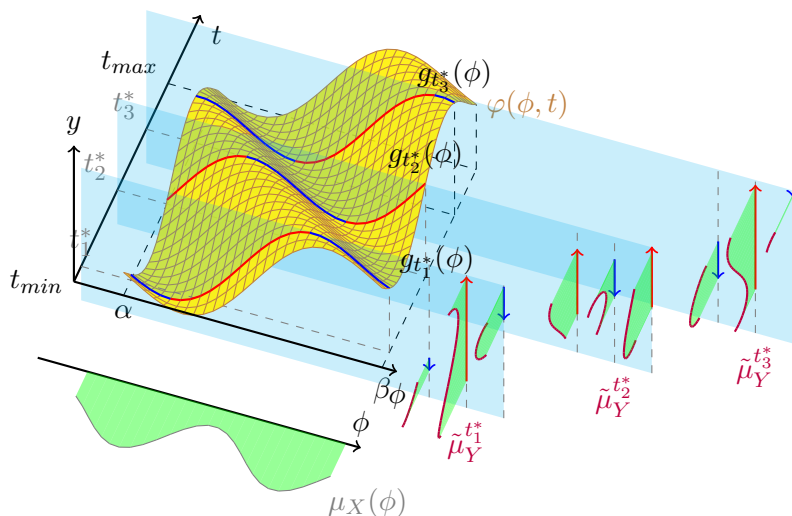


Figure 8: The physical system $\varphi(\phi, t) = k \cdot \varphi + A \cos(\omega t + \phi)$ and the *folding-domain function* approach.

Following Section 2.1, the procedure starts by replacing the description of the physical system given by $\varphi(\phi, t)$, for each $t \in [0, t_{max}]$, with:

1. the point $\chi_0(t) := \varphi(\alpha, t)$, corresponding to $g(\alpha_0) = g(\alpha) = g_t(\alpha)$,
2. the vector Λ_t that contains the arrows,

3. the function η_t ,
4. according to (2.3), the functions $u_{i,t}(y)$, (with $i \in \{\rho_1, \dots, \rho_{p_t}(y)\} = I_t(y)$), which associate all the values $u_{\rho_1}, \dots, u_{\rho_{p_t}}$ to each point y in the physical space, such that $\eta_t(u_i) = \phi_i$ and $\varphi(\phi_i, t) = y$.

We further notice that the bijection $\eta_{t_i^*}$ allows us to associate a probability weight $\tilde{\mu}_Y$ to each point on the three arrows via the PDF μ_X : indeed, in Figure 8, at the right-hand side, we show the graphs of three groups (for $t = t_1^*, t_2^*, t_3^*$) of three functions (over three arrows). We recall that we have denoted these three groups of functions (the so-called unfolded intermediate) as $\tilde{\mu}_Y^t$, with $t = t_1^*, t_2^*, t_3^*$. These three plots have been produced as a composition of μ_X with the inversions of $g_{t_i^*}$ in each of the three intervals of monotonicity in which the domain of μ_X is split. This can be obtained by choosing a point $u \in [0, S_{\Lambda_{t_i^*}}]$ and then by computing $\mu_X[\eta_{t_i^*}(u)]$. We stress that these composite graphs are represented just for the sake of intuitively describing the underlying idea. The real graphs of μ_Y should take into account a scaling factor given by the inverse derivative and should be overlapped by the unfolding, summing up the different layers, according to (2.4).

The graphs of functions η_t are plotted in Figure 9. In both Figures 8 and 9 we consider three cases $t = t_1^*, t_2^*, t_3^*$ for which the same idea can be applied.

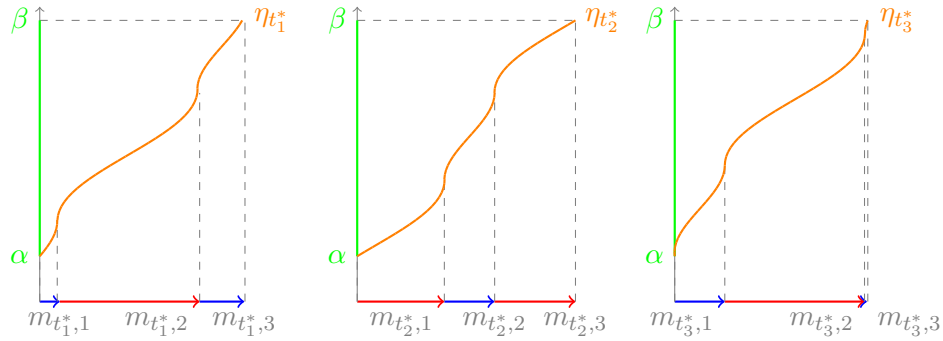


Figure 9: The functions $\eta_{t_1^*}$, $\eta_{t_2^*}$ and $\eta_{t_3^*}$ for different values of $t_1^* < t_2^* < t_3^*$.

Now we conclude this section providing an heuristic derivation of the PDF $\mu_Y = \psi(y, t)$. Let y be a point of the physical space where it exists a probability of finding the system, with respect to the random variable ϕ . The PDF $\psi(y, t)$ is obtained by determining all the points $\phi_i(y) \in [\alpha, \beta]$ such that $\varphi(\phi_i(y), t) = y$. Indeed, we expect that the probability of finding the system in y at time t can be obtained as the sum of the probabilities of all the values of $\phi_i(y)$ that will make the system to be in the position y at the time t . The subintervals within $[\alpha, \beta]$ where these $\phi_i(y)$ are located, are determined by the set of indexes $I_t(y)$. This is due to the fact that $\varphi(\phi, t)$ is *spreading* the mass probability μ_X

around in the image space. In Figure 10 we show the regions where overlap will occur (darker green). In turn, in Figure 11 we show how this overlap will displace the resulting probability. For simplicity, however, in this later figure we have disregarded the Jacobian of the transformation in the summation of the different parts. However, this Jacobian is an essential part in the transformation as φ squeezes or stretches the probability mass $\mu(\phi)$ in the final space. This deformation also affects the final PDF ψ through the derivative (Jacobian) in (2.4). For example, when y corresponds to a local minimum or local maximum value of $\varphi(\phi, t)$, we expect a *peak of probability*. Indeed the derivative $\partial\varphi/\partial\phi$ is zero and then the derivative of the corresponding inverse auxiliary function η_t is infinity.

In summary, the main idea behind the FDF approach can be sketched in following scheme:

$$\begin{aligned}
y &\xrightarrow{u_{i,t}} \{u_{\rho_1}, \dots, u_{\rho_{p_t}}\} \xrightarrow{\eta_t} \{\phi_i : i \in I_t(y)\} \xrightarrow{\mu_X} \dots \\
&\dots \xrightarrow{\mu_X} \{\mu_X(\phi_i) : i \in I_t(y)\} \xrightarrow{\Sigma} \sum_{i \in I_t(y)} \mu_X(\phi_i(y)) \cdot \frac{d\eta_t}{du}(u_i),
\end{aligned} \tag{3.3}$$

where we recall that $\phi_i = \eta_t(u_i)$ for each $i \in I_t(y)$.

We want to emphasize that the FDF approach presents several advantages from the point of view of numerical implementation of an algorithm aiming at the RVT. In particular,

1. $u_{i,t}(x)$ is piecewise linear,
2. $\eta_t(u)$ is invertible,
3. both of these functions can be very easily determined numerically.

All these facts permits the use of an algorithm which is not based on the reconstruction of the final probability via the generation of bundles of trajectories, using the Monte Carlo method, and calculating the final probability through a histogram. Instead, the piece-wise nature of our approach allows us to construct the final solution through a more effective piece-wise analysis.

4. The algorithm

In this section we present the application of the Folding Domain Function algorithm (FDF) to some cases of interest, in order to check its consistency by comparison with a brute force algorithm. As before, the dynamical system has a collection of solutions described by the function $\varphi(\phi, t)$, which parametrically depends on the random variable ϕ . In most of the cases of interest, such a solution can not be determined analytically and, therefore, approximations to the solution are generated *via Numerical integrators*².

²In our examples we have used those already implemented in the program Octave [13].

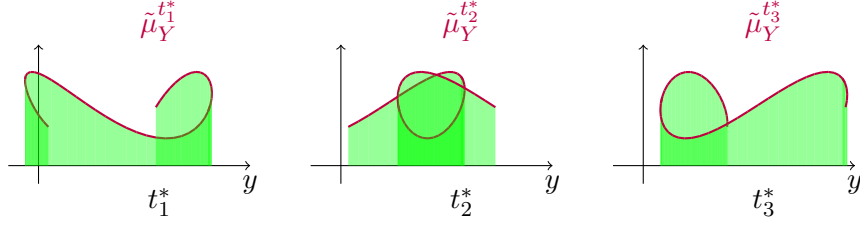


Figure 10: Here we have $t = t_1^*$, $t = t_2^*$ and $t = t_3^*$. We notice that $I_{t_1^*}(y) = \{1, 2\}$, $I_{t_1^*}(y) = \{2\}$ and $I_{t_1^*}(y) = \{2, 3\}$ as y varies from the $g_{t_1^*, \min}$ to $g_{t_1^*, \max}$. Similarly, the three cases of $t = t_2^*$ as y varies, are $I_{t_1^*}(y) = \{1\}$, $I_{t_1^*}(y) = \{1, 2, 3\}$ and $I_{t_1^*}(y) = \{3\}$. Finally, the three cases of $t = t_3^*$ as y varies, are $I_{t_1^*}(y) = \{1, 2\}$, $I_{t_1^*}(y) = \{2\}$ and $I_{t_1^*}(y) = \{2, 3\}$.

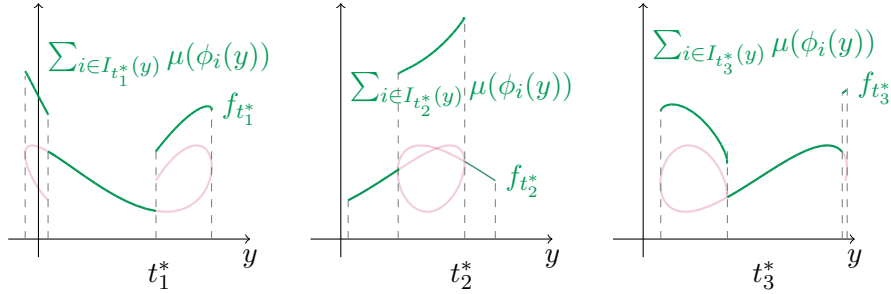


Figure 11: Functions $f_{t_1^*}^*$, $f_{t_2^*}^*$ and $f_{t_3^*}^*$. The graphs are obtained with $f_t = \sum_{i \in I_t(y)} \mu(\phi_i(y))$ for each $t \in \{t_1^*, t_2^*, t_3^*\}$. The function f_t represent the additive components in the last part of the formula (3.3) without the multiplicative factor $\frac{d\eta_t}{du}$.

4.1. The brute force algorithm

The algorithm based on the Monte Carlo generation of instances of the RV ϕ will be referred to as the *brute-force* algorithm. We use this method for comparison with the FDF results and is described in the following list the steps:

1. We numerically generate a large number of points $\phi \in [\alpha, \beta]$ distributed according to the known PDF $\mu : [\alpha, \beta] \rightarrow \mathbb{R}_{\geq 0}$. Typically, computers provide uniform as well as Gaussian random number generators, which could be used at this point to generate any general distribution function μ for the random number ϕ , provided that the latter is well behaved.
2. For each $\phi \in [\alpha, \beta]$ and a given time t , we calculate the value $\varphi(\phi, t)$
3. Given the mapping $y = \varphi(\phi, t)$, we numerically estimate the PDF $\psi(y)$ from a given histogram constructed from the randomly generated trajectories.

4. Finally the histogram needs to be properly normalized.

4.2. The FDF-algorithm

Here we will use x rather than ϕ as a random variable, to stress the fact that the theory also works for non-invertible functions, which are not solutions of any RDE. We will restrict the use of ϕ for the cases where the mapping is obtained from a RDE. Again, for mappings arising from RDE, the function $g(x) = \varphi(\phi, t)$, in agreement with the notation of Section 2.

In the following, we list the steps of the FDF algorithm:

1. First of all we split the interval $[\alpha, \beta]$ into $N := N_{\text{div}}$ subintervals of equal length and set

$$x_i := \alpha + i \frac{\beta - \alpha}{N}, \quad i = 0, \dots, N,$$

so that $\alpha = x_0$ and $\beta = x_N$. Then we compute the image values $g(x_i)$ either analytically or numerically.

2. Next, we consider the indexes $i \geq 1$ such that

$$(g(x_i) - g(x_{i-1}))(g(x_{i+1}) - g(x_i)) \leq 0. \quad (4.1)$$

Clearly, if i is such that the above relation is satisfied, then an extremum point of g is contained in the open interval $]x_{i-1}, x_{i+1}[$ and it will be approximated by x_i . These, together with α and β are the points α_j in Section 2.1.

The algorithm saves the $(k+1)$ -tuple $(\alpha_j)_{j=0, \dots, k}$, the values $g(\alpha_j)$, together with the set of j -indices is the set of i 's such that (4.1) holds. At this point, also the vector $\Lambda = (\lambda_1, \dots, \lambda_k)$ and the $(k+1)$ -tuple $(m_j)_{j=0, \dots, k}$ are determined, together with the range $[g_{\min}, g_{\max}]$ of the function g .

3. In order to produce the ordered set $B = \{b_0, \dots, b_\ell\}$ with $g_{\min} = b_0 < b_1 < \dots < b_\ell = g_{\max}$, we sort the values $g(\alpha_j)$ in increasing order and erase the possible repeated values (if any). At this step, also the central points $c_i = \frac{b_{i-1} + b_i}{2}$ are determined and then find the set of indices $I(c_i) = I(y)$, for all $y \in]b_{i-1}, b_i[$. In fact, we have that $j \in I(c_i)$ if and only if

$$0 < (c_i - g(\alpha_{j-1}))\text{sign}(\lambda_j) < |\lambda_j|,$$

according to (2.2). This procedure allows to save the set $I(c_i)$. In a similar manner, we determine the sets $I(b_i)$.

4. The function η is approximated with a piecewise linear interpolant passing through the points $(\hat{g}(x_i), x_i)$ where the values $\hat{g}(x_i)$ are computed using (2.1).

5. As a last step, we divide each interval $[b_{i-1}, b_i]$ into a finite number of parts with a fixed step-size Δ (in this manner the larger intervals are divided into larger parts than the smaller ones). Then, knowing the sets $I(b_{i-1}), I(c_i), I(b_i)$ and using (2.3), we can determine the values $u_{\rho_1}(y), \dots, u_{\rho_p}(y)$ (with $\{\rho_1, \dots, \rho_p\} = I(y)$), for each y in the Δ -partition of $[b_{i-1}, b_i]$. From these points we find the images $\eta(u_{\rho_1}(y)), \dots, \eta(u_{\rho_p}(y))$ in $[\alpha, \beta]$ and finally we can easily compute

$$\mu_Y(y) = \sum_{i \in I(y)} \mu_X(\eta(u(y))) \frac{d\eta}{du}(u(y)).$$

Observe that, in the algorithm, the derivative of η , can be easily obtained either with the absolute value of $1/g'\eta(u(y))$ (when the analytic expression of g is known), or by a standard approximation of the incremental ratio of g computed by a subroutine in the differential equation solver.

5. Numerical results

In this section we provide some numerical experiments that show the feasibility and reliability of our theory. For the initial random variable X , let us choose the non-uniform, non-gaussian density function

$$\mu_X(x) = \frac{\sin(\omega x) + 2}{\int_{\alpha}^{\beta} (\sin(\omega x) + 2) dx}, \quad \omega = 5. \quad (5.1)$$

which we will use the same for all the examples. Clearly, $\mu_X(x) \geq 0$ for all $x \in [\alpha, \beta]$ and $\int_{\alpha}^{\beta} \mu_X(x) dx = 1$.

5.1. Example (a)

As a first example, we analyze the logistic map $L(x) = rx(1-x)$, described in the case (a) in the Introduction, and study the third iterate $g(x) := L^{(3)}(x)$, which is analogous to fixing a final time in a physical map, although this example is a case in which the mapping is not created from a RDE. We thus brush the interval of initial values $x \in [\alpha, \beta]$ to generate the function $g(x)$. In agreement with the case presented in Figure 1, we take $r = 3.9$. The natural domain is then the interval $[\alpha, \beta] = [0, 1]$. Moreover, $g_{\min} = 0$ and $g_{\max} = L(1/2) = r/4 = 0.975$. For the simulation, we have chosen $N = N_{\text{div}} = 400$.

Figure 12 shows the density μ_X and the function g . Figure 13 shows the function η (which is the inverse of \hat{g}) and the resulting density function μ_Y , produced numerically via both the brute-force technique and the FDF-A, for comparison. It is apparent from the figure that our approach provides a smoother, more precise outcome than the brute-force one. Also very important is that with the FDF-A the computational cost is remarkably reduced. This is particularly relevant when the number of iterates is very large. In the Monte Carlo approach, the generation of the bundle of trajectories may become a computationally very intensive task.

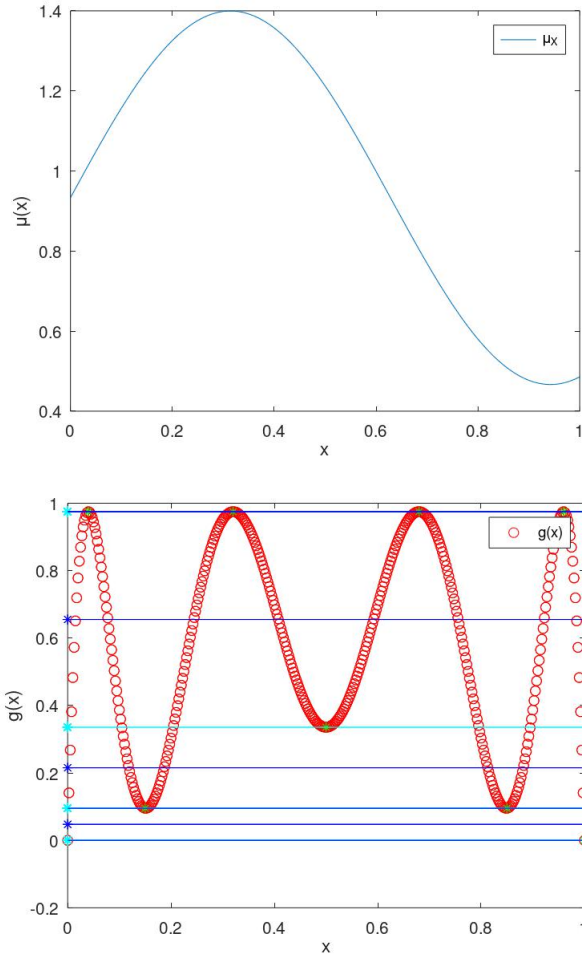


Figure 12: For the above set of parameters, we consider the density function μ_X (upper panel) and the function g (lower panel). In the graph of function g we have marked, on the vertical axis, the points b_0, \dots, b_ℓ , making the set B (of four points), together with the three middle points c_i . From the figure, the meaning of Lemma 2.2 is evident.

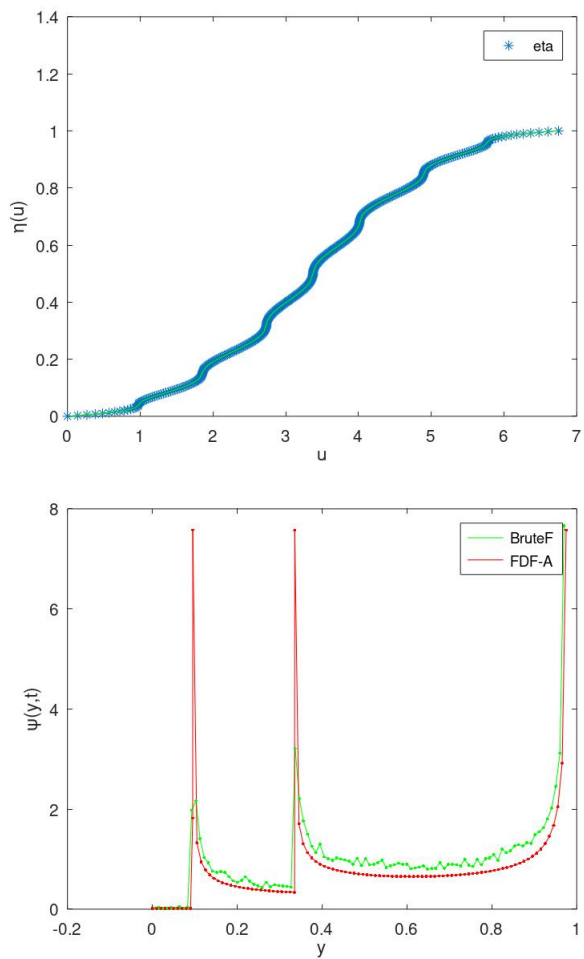


Figure 13: The function η (upper panel) and the density function μ_Y (lower panel). For the density function we compare two different graphs obtained, respectively, by the brute-force algorithm (in green) and by the FDF-A (in red).

5.2. Example (b)

As a second example, we consider a projection of the Poincaré map associated with the shooting method applied to a second-order scalar equation of Duffing type $x'' + \rho(x) = 0$. With reference to the two cases introduced in Figure 2 and Figure 3, we study the “classical” Duffing equation with $\rho(x) = 4x^3$ and the pendulum equation with $\rho(x) = \sin(x)$.

For the former case, we take as reference time-interval $[0, T_{\max}] = [0, 5]$ and solve the initial value problems

$$\begin{cases} y' = v, & v' = -4y^3 \\ y(0) = 0, & v(0) = \phi \end{cases} \quad (5.2)$$

on the interval $[0, T_{\max}]$, to obtain the function $\phi \mapsto y(t, \phi)$ for $t = T_{\max}$ (cf. Figure 2, lower panel). To solve numerically (5.2) we use an already implemented ODE-solver of Octave [13], with a step-size $5/300$. The chosen density function μ_X is the same as in (5.1) for the interval $[\alpha, \beta] = [0, 5]$. Moreover, $g_{\min} \approx -1.3015$ and $g_{\max} \approx 1.6717$. For the simulation, we have chosen $N = N_{\text{div}} = 300$.

Figure 14 shows the density μ_X and the function $g(x) = y(t, x)$. Figure 15 shows the function η and the resulting density function μ_Y , numerically produced via the brute-force technique and also through the FDF-A.

Again, the results obtained with the FDF algorithm are smoother, more accurate and are produced at lower computational cost than with the brute-force algorithm.

Considering now the case of the pendulum equation, we take as reference time-interval $[0, T_{\max}] = [0, 18]$ and solve the initial value problems

$$\begin{cases} y' = v, & v' = -\sin(y) \\ y(0) = 0, & v(0) = \phi \end{cases} \quad (5.3)$$

on the interval $[0, T_{\max}]$, obtaining the function $\phi \mapsto y(t, \phi)$ for $t = T_{\max}$ (cf. Figure 3, right panel). To solve numerically (5.3) we use, as in the above example, an already implemented ODE-solver of Octave [13], with a step-size $18/200$. The chosen density function μ_X is the same as in (5.1) for the interval $[\alpha, \beta] = [0, 1.99]$. Moreover, $g_{\min} \approx -2.5019$ and $g_{\max} \approx 2.9224$. For the simulation, we have chosen $N = N_{\text{div}} = 200$.

Figure 16 shows the density μ_X and the function $g(x) = y(t, x)$.

Figure 17 shows the function η and the resulting density function μ_Y , produced, numerically, via the brute-force technique and the FDF-A.

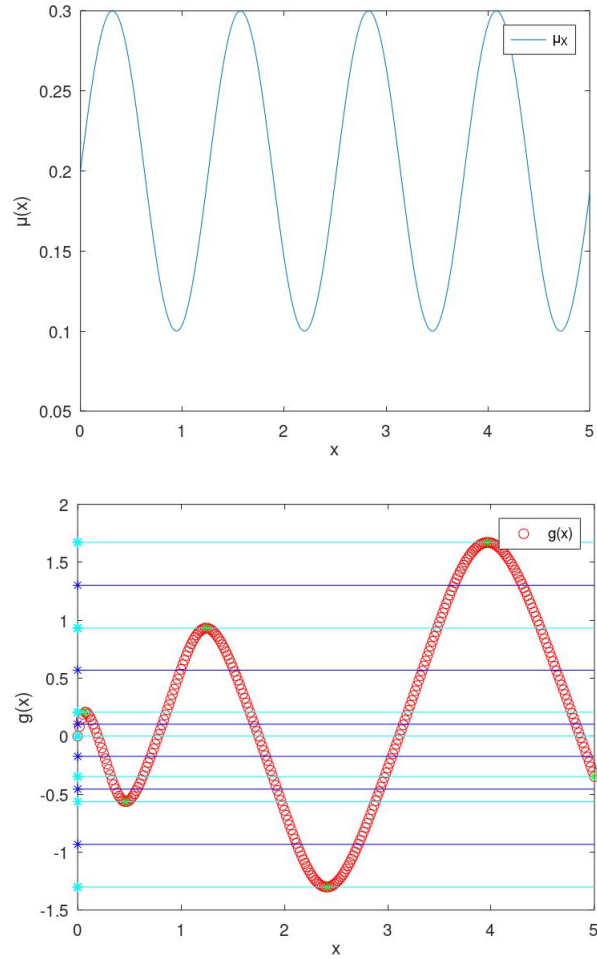


Figure 14: For the above set of parameters, we consider the density function μ_X (upper panel) and the function g (lower panel). In the graph of function g we have marked, on the vertical axis, the points b_0, \dots, b_ℓ , making the set B (of seven points), together with the six middle points c_i .

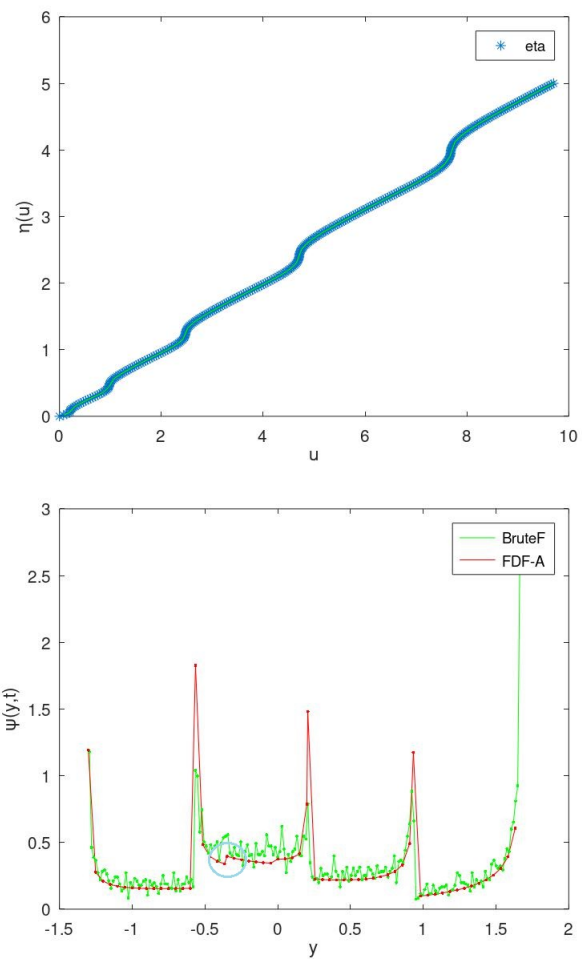


Figure 15: The function η (upper panel) and the density function μ_Y (lower panel). For the density function we compare two different graphs obtained, respectively, by the brute-force algorithm (in green) and by the FDF-A (in red).

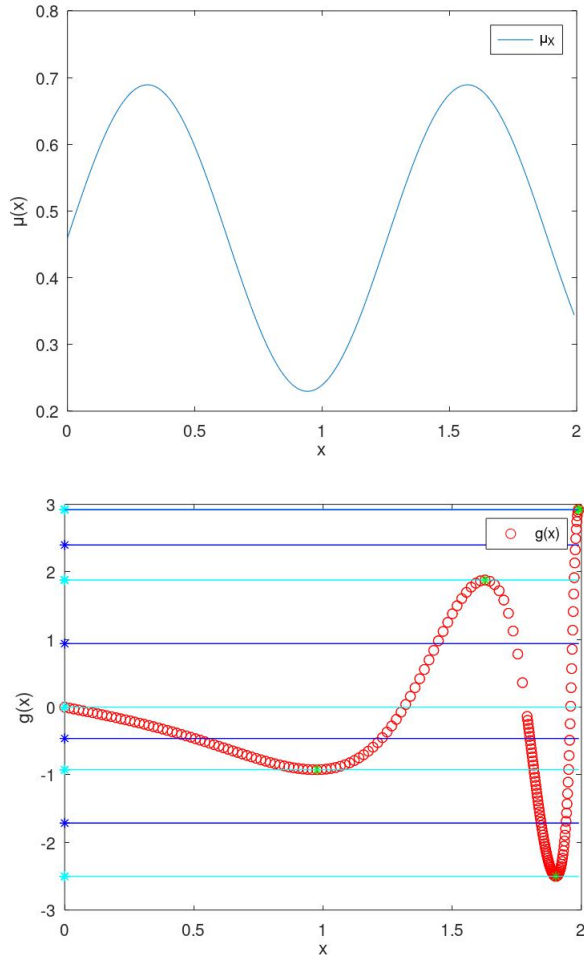


Figure 16: For the above set of parameters, we consider the density function μ_X (upper panel) and the function g (lower panel). In the graph of function g we have marked, on the vertical axis, the points b_0, \dots, b_ℓ , making the set B (of five points), together with the four middle points c_i .

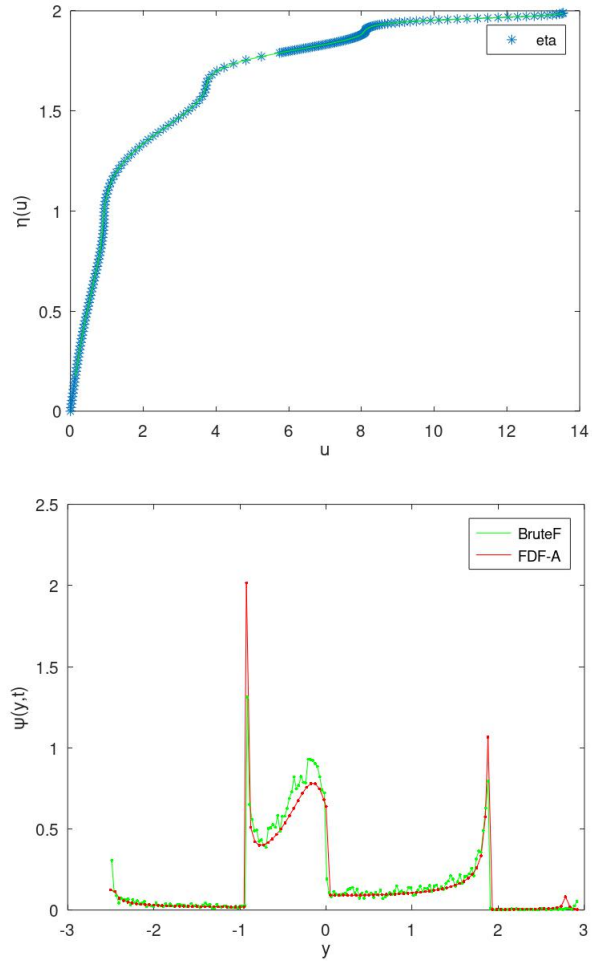


Figure 17: The function η (upper panel) and the density function μ_Y (lower panel). For the density function we compare two different graphs obtained, respectively, by the brute-force algorithm (in green) and by the FDF-A (in red).

5.3. Example (c)

As a third example, we consider the problem in (1.9), leading to an explicit form for $\varphi(\phi, t)$ as in (1.10). In this case, we have an explicit known form for the function

$$g(x) = kx + A \cos(\omega t + x), \quad (5.4)$$

where, k, A, ω, t are fixed parameters for our numerical simulation. The chosen density function μ_X is the same as in (5.1) for the interval $[\alpha, \beta] = [2, 4]$. For the simulation, we have chosen $N = N_{\text{div}} = 200$.

Figure 18 shows the density μ_X and the function g , with g defined for the parameters $k = 1, A = 2, \omega = 6$ and $t = 1$.

Figure 19 shows the function η (which is the inverse of \hat{g}) and the resulting density function μ_Y , via the brute-force procedure as well as the FDF-A.

Finally, we want to point out the small jumps present in Figure 15 and Figure 19 which we have highlighted with a small circle. These discontinuities are due neither to numerical errors nor to any flaw in the FDF algorithm. Instead, they reflect the complexity of the overlapping of different branches in the folded domain, as we have shown in the sketch of Figure 11. In this particular case, they are due to the overlapping of the extremal points $g(\alpha)$ and/or $g(\beta)$ with other values in the image set $g([\alpha, \beta])$.

6. Conclusion and future work

In the present paper we have addressed a classical problem in the study of random variables, namely, quoting [15, p.80]: *Let X be a RV with density f . Suppose $Y = g(X)$. Can we express the density of Y (if it exists), in terms of f ?* If X has a continuous density function and g is piecewise strictly monotone and continuously differentiable, the problem is solved, from a theoretical point of view, by the formula

$$\mu_Y(y) = \sum_{i=1}^n \mu_X(h_i(y)) |h'_i(y)| \mathbb{1}_{\wedge}(y) \quad (6.1)$$

(see [15, Corollary 11.3]). In (6.1), \wedge denotes the range of g and it is assumed that there exists intervals I_1, I_2, \dots, I_n which partition the domain of g and such that g is strictly monotone and continuously differentiable on the interior of each I_i . Then, $h_i : g(I_i) \rightarrow I_i$ denotes the inverse of g restricted to I_i . In applying the above formula, one has to decide for every y in the range of g the correct functions h_i to be chosen in the summation. In the simplest case, g is continuously differentiable with non-vanishing derivative, and the above formula reduces to

$$\mu_Y(y) = \mu_X(h(y)) |h'(y)|, \quad \text{for } h = g^{-1} \quad (6.2)$$

(see [15, Corollary 11.2]). This latter result may be easily extended to the vector case; in this situation, one has to assume that g is a diffeomorphism.

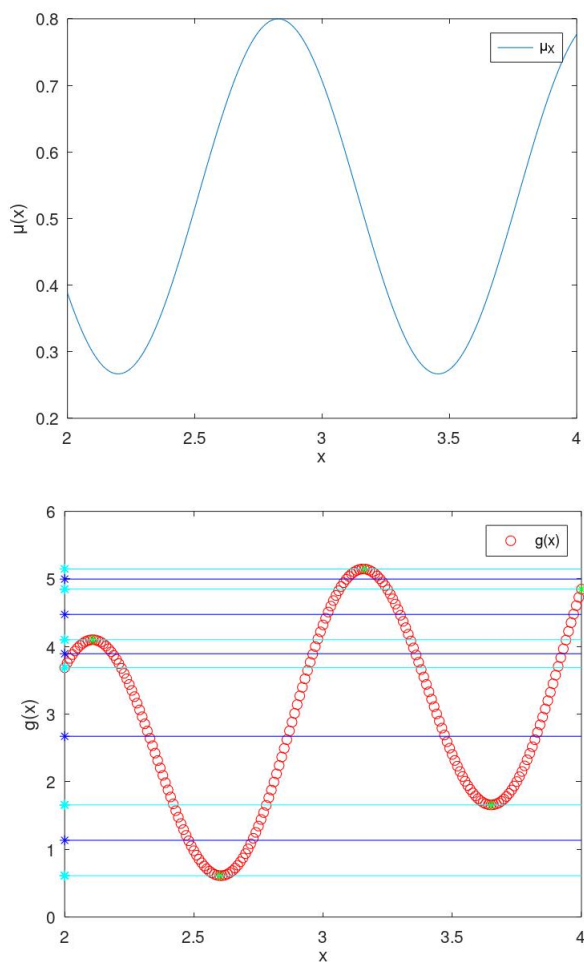


Figure 18: We consider the density function μ_X (upper panel) and the function g (lower panel). In the graph of function g we have marked, on the vertical axis, the points b_0, \dots, b_ℓ , making the set B (of six points), together with the five middle points c_i . From the figure, the meaning of Lemma 2.2 is evident.

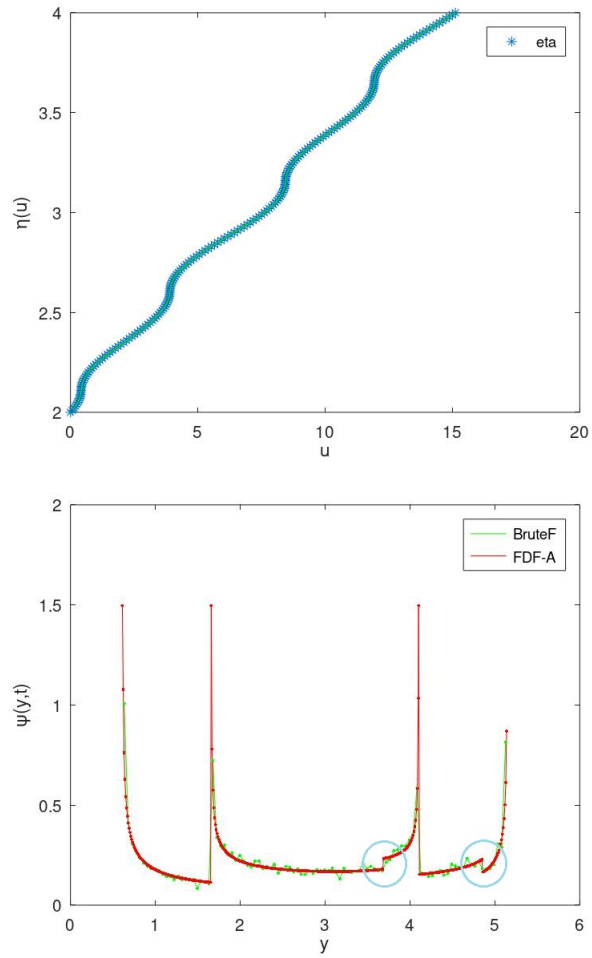


Figure 19: The function η (upper panel) and the density function μ_Y (lower panel). For the density function we compare two different graphs obtained, respectively, by the brute-force algorithm (in green) and by the FDF-A (in red). It is apparent that our approach provides a smoother and more precise outcome than the other one. Moreover, with the FDF-A the computational cost is remarkably reduced.

Applications of (6.2) for one-dimensional and higher-dimensional models have received a great deal of interest in the past decades, as witnessed by a growing list of published research articles in this area in recent years (see, for instance, Refs. [5, 6, 9, 8, 7, 10, 11]). Actually, the implementations of (6.2) in applied mathematical models is usually referred to as *Probabilistic Transformation Methods* (according to Kadry in [16]) or *Random Variable Transformation (RVT) Technique* (according to Casabán et al. in Ref. [9] and also to the more recent work by Cortés et al. [12]). Further applications of this method have been developed for various mathematical model equations of great interest for ecological and biological sciences in subsequent articles, as those cited above. In some of these articles (as, for instance, in Ref. [8]) the domain of the inverse transformation is split into two disjoint open intervals, so that (6.1) simplifies to equation (6.2) applied twice. In the very recent work [1], Almalki, Elshekhiy and Almutairi deal with a very general case of non-monotone transformation g and study the probability distribution of $Y = g(X)$ from a theoretical and numerical point of view.

Our work, independently follows a similar line of reasoning, namely, to obtain information of the RV $Y = g(x)$, under the most general assumptions for g . With this respect, our main contributions in the present work are the following:

- As already observed, in applying the formula (6.1), one has to decide *for every y in the range of g* the correct functions h_i to choose in the summation. With our approach (and using Lemma 2.1 and Lemma 2.2) rather we can easily determine the index set $I(y)$ associated with y ;
- We have proposed a new method to obtain the piecewise-partial inverses h_i of g , by introducing a unique global function η . The function η , in some sense, “unfolds” the graph of g in a manner such that the derivatives (in absolute value) $|h'_i(y)|$ in (6.1) correspond to the inverse derivative of η computed in different intervals.
- Our approach is mathematically rigorous, because we can independently re-establish (6.1), passing through the use of the function η (see Section 2.1);
- Our method, when numerically implemented, requires a minimal set of information and therefore is extremely simple and fast compared to standard histogram methods based on a Monte Carlo sampling of the initial probability distribution.

The very recent articles [1, 12, 17, 20] show the persistent interest and relevance of the problem considered in this work, both from the theoretical and the applied point of view. We hope that our contribution can provide a new tool in this area of research.

As a final comment, we outline some possible extensions of our approach to the higher-dimensional case. Let X be a m -dimensional random variable with domain \mathcal{D}_X and let $g : \mathbb{R}^m \rightarrow \mathbb{R}^m$ be continuously differentiable mapping, leading to the new Random Variable $Y = g(X)$, with values in \mathbb{R}^m . As in the one-dimensional case, we are interested in providing an efficient method to estimate the probability density function μ_Y in terms of μ_X .

From a theoretical point of view, the problem is solved by [15, Corollary 12.1]; however, implementing the method in concrete examples may be a formidable task. This is therefore a problem of great interest, as witnessed by the recent articles [20, 17]. As Lemma 2.1 and Lemma 2.2 can be proven to be also valid in more than one dimension, our algorithm can be extended to maps connecting higher dimensional spaces (see also Remark 2.1). On the other hand, while in the one-dimensional case, the singular set reduces to a finite (discrete) set of points, in dimension $m \geq 2$, we have to face some complex differential geometry problems concerning the boundaries of the sets where g is partially invertible. This problem will be addressed next.

CRediT authorship contribution statement

Fabrizio Masullo: Conceptualization, Formal analysis, Methodology, Software, Visualization, Organization of the article. **Fabio Zanolin:** Formal analysis, Organization of the article. **Josep Bonet Avalos:** Supervision, Research Project Leader.

Conflict of interest

The authors claim that there is no conflict of interest associated with this article and with the research leading to this article.

References

- [1] N. H. Almalki, A. A. Elshekhiy, and I. S. Almutairi. A numerical modeling and its computational implementing simulation for generating distributions of the complicated random variable transformations with applications. *Appl. Numer. Math.*, 186:274–288, 2023.
- [2] A. Ambrosetti and G. Prodi. *A primer of nonlinear analysis*, volume 34 of *Cambridge Studies in Advanced Mathematics*. Cambridge University Press, Cambridge, 1995. Corrected reprint of the 1993 original.
- [3] L. Arnold. *Random dynamical systems*. Springer Monographs in Mathematics. Springer-Verlag, Berlin, 1998.
- [4] F. Balibrea, T. Caraballo, P. E. Kloeden, and J. Valero. Recent developments in dynamical systems: three perspectives. *Internat. J. Bifur. Chaos Appl. Sci. Engrg.*, 20(9):2591–2636, 2010.
- [5] C. Burgos, J. Calatayud, J.-C. Cortés, and A. Navarro-Quiles. A full probabilistic solution of the random linear fractional differential equation via the random variable transformation technique. *Math. Methods Appl. Sci.*, 41(18):9037–9047, 2018.

- [6] J. Calatayud, J. C. Cortés, F. A. Dorini, and M. Jornet. Dealing with variability in ecological modelling: an analysis of a random non-autonomous logistic population model. *Math. Methods Appl. Sci.*, 45(6):3318–3333, 2022.
- [7] M.-C. Casabán, J.-C. Cortés, A. Navarro-Quiles, J.-V. Romero, M.-D. Roselló, and R.-J. Villanueva. A comprehensive probabilistic solution of random SIS-type epidemiological models using the random variable transformation technique. *Commun. Nonlinear Sci. Numer. Simul.*, 32:199–210, 2016.
- [8] M.-C. Casabán, J.-C. Cortés, A. Navarro-Quiles, J.-V. Romero, M.-D. Roselló, and R.-J. Villanueva. Probabilistic solution of the homogeneous Riccati differential equation: a case-study by using linearization and transformation techniques. *J. Comput. Appl. Math.*, 291:20–35, 2016.
- [9] M.-C. Casabán, J.-C. Cortés, J.-V. Romero, and M.-D. Roselló. Determining the first probability density function of linear random initial value problems by the random variable transformation (RVT) technique: a comprehensive study. *Abstr. Appl. Anal.*, pages Art. ID 248512, 25, 2014.
- [10] M.-C. Casabán, J.-C. Cortés, J.-V. Romero, and M.-D. Roselló. Solving random homogeneous linear second-order differential equations: a full probabilistic description. *Mediterr. J. Math.*, 13(6):3817–3836, 2016.
- [11] J.-C. Cortés, S. K. El-Labany, A. Navarro-Quiles, M. M. Selim, and H. Slama. A comprehensive probabilistic analysis of approximate SIR-type epidemiological models via full randomized discrete-time Markov chain formulation with applications. *Math. Methods Appl. Sci.*, 43(14):8204–8222, 2020.
- [12] J.-C. Cortés, E. López-Navarro, J.-V. Romero, and M.-D. Roselló. Probabilistic analysis of a cantilever beam subjected to random loads via probability density functions. *Comput. Appl. Math.*, 42(1):Paper No. 42, 32, 2023.
- [13] J. W. Eaton, D. Bateman, S. Hauberg, and R. Wehbring. *GNU Octave version 7.3.0 manual: a high-level interactive language for numerical computations*, 2022.
- [14] J. K. Hale. *Ordinary differential equations*. Robert E. Krieger Publishing Co., Inc., Huntington, N.Y., second edition, 1980.
- [15] J. Jacod and P. Protter. *Probability essentials*. Universitext. Springer-Verlag, Berlin, 2000.
- [16] S. Kadry. On the generalization of probabilistic transformation method. *Appl. Math. Comput.*, 190(2):1284–1289, 2007.

- [17] G. La Valle, R. Laudani, and G. Falsone. Response probability density function for non-bijective transformations. *Commun. Nonlinear Sci. Numer. Simul.*, 107:Paper No. 106190, 9, 2022.
- [18] T. Y. Li and J. A. Yorke. Period three implies chaos. *Amer. Math. Monthly*, 82(10):985–992, 1975.
- [19] J. D. Murray. *Mathematical biology. I*, volume 17 of *Interdisciplinary Applied Mathematics*. Springer-Verlag, New York, third edition, 2002. An introduction.
- [20] A. Navarro-Quiles, R. Laudani, and G. Falsone. A new stochastic method based on the Taylor expansion to compute response probability densities of uncertain systems. *Internat. J. Numer. Methods Engrg.*, 124(5):1111–1127, 2023.
- [21] A. Papoulis. *Probability, random variables, and stochastic processes*. McGraw-Hill Series in Electrical Engineering. Communications and Information Theory. McGraw-Hill Book Co., New York, second edition, 1984.
- [22] T. T. Soong. *Random differential equations in science and engineering*. Mathematics in Science and Engineering, Vol. 103. Academic Press [Harcourt Brace Jovanovich, Publishers], New York-London, 1973.